AIAA JOURNAL
Vol. 40, No. 4, April 2002

Unsteady Force on Slender Aircraft with Free Vortices in Inviscid Flow

T. W. G. de Laat*
Royal Netherlands Military Academy, 4800 PA Breda, The Netherlands
and
R. Coene†
Delft University of Technology, 2629 HS Delft, The Netherlands

Expressions are derived for the force on circular and wing-body contours induced by a vortex pair in a two-dimensional uniform unsteady inviscid flow, such as arise in the slender-body approximation of an aircraft. Zero-force curves for the classical vortex pair behind a circular cylinder in oncoming flow are found, and it is shown that the direction of the force can be upwind as well as downwind. A convenient expression for the force on a contour in a symmetric flowfield is obtained by conformal mapping, involving only the first- and second-order derivatives of the required transformation-function. A result of practical interest for free vortices intended to enhance the lift force of an aircraft is that the force on the crossflow contour induced by vortices with a certain strength generally decreases when enlarging the width of the contour perpendicular to the direction of that force. So span reduction increases the lift generated by vortices above the wings. The position of the vortices in relation to the contour is critical, however, as there are areas that are shown, where the lift caused by the vortices is negative. The force caused by the symmetric vortex pair on the symmetric contour is independent of the speed of the oncoming flow; the pressure distribution on the contour, however, does vary with changing speed of the oncoming flow.

Nomenclature

a	=	circle radius
c	=	circle radius of the body of the wing-body configuration
c_{F_y}	=	$F_y/\frac{1}{2}\rho w^2 2a$
F_x	=	force component in x direction
F_y	=	force component in y direction
f	=	frequency
i^2	=	-1, imaginary unit
p	=	pressure
$p_{\frac{1}{2}\rho v\cdot v}$	=	pressure from the $\frac{1}{2}\rho \boldsymbol{v}\cdot\boldsymbol{v}$-part of the Bernoulli equation
$p_{\rho(\partial\phi/\partial t)}$	=	pressure from the $\rho(\partial\phi/\partial t)$ part of the Bernoulli equation
r	=	radial coordinate
r_1	=	radial coordinate of vortex number 1
s	=	wing span
T	=	cycle time
t	=	time
u_1	=	velocity component in x direction of vortex number 1
V	=	airspeed
$\boldsymbol{v}$	=	$\boldsymbol{v}(x, y)$ velocity vector in the crossflow plane
v_1	=	velocity component in y direction of vortex number 1
w	=	upwash in slender body approach: $w = V\sin\alpha$
x	=	real part of complex variable z, x coordinate
y	=	imaginary part of complex variable z, y coordinate
$\bar{z}$	=	$x - yi$, complex conjugate of z
z_1	=	$x_1 + y_1 i = r_1 e^{\theta_1 i}$, complex coordinate of vortex number 1
$\dot{z}_1$	=	$\mathrm{d}z_1/\mathrm{d}t = u_1 + v_1 i$, complex velocity of vortex number 1
α	=	angle of attack
Γ	=	vortex strength
Γ_1	=	strength of vortex number 1
ζ	=	$\xi + \eta i$, complex coordinate in ζ plane
ζ_1	=	complex coordinate of vortex number 1 in ζ plane
ζ_1'	=	$(\mathrm{d}\zeta/\mathrm{d}z)_{z=z_1}$
ζ_1''	=	$(\mathrm{d}^2\zeta/\mathrm{d}z^2)_{z=z_1}$
η	=	imaginary part of complex coordinate ζ
θ	=	angular coordinate
θ_1	=	angular coordinate of vortex number 1
ξ	=	real part of complex coordinate ζ
ρ	=	air density
ϕ	=	real part of potential flow function χ
χ	=	complex potential flow function, $\chi = \phi + \psi i$
ψ	=	stream function, imaginary part of complex potential flow function χ

I. Introduction

THE force on an aircraft from free vortices is important to improve maneuverability (e.g., Ref. 1). The slender-body approximation of an aircraft with free vortices approximately parallel to its body yields a two-dimensional crossflow field with vortex filaments (e.g., Ref. 2). The vortices might be formed by strakes, canard wings, or at the forebody as a result of flow detachment or might be present from the wake of another aircraft.[3] This paper is mainly concerned with vortices generated at strakes, canard wings or at the forebody, which are intended to generate extra lift force on the wing or body surface over which they are positioned. We are especially interested in the effect on the aircraft lift of the vortex position above the wing-body combination. The position of the vortices is dependent on the forebody, canard-wing, or strake-position and width and can be influenced during the design process. The aerodynamic forces acting on bodies are routinely calculated these days using computer codes solving the Navier–Stokes equations for any geometry in time-dependent flows (e.g., Ref. 4). However the knowledge of special inviscid potential flow features of vortices provides insight, which is helpful in the design process of an aircraft or missile when planning

Received 30 January 2001; revision received 30 August 2001; accepted for publication 10 September 2001.

*Assistant Professor, P.O. Box 90002, De la Reyweg 95; twg.d.Laat@mindef.nl. Member AIAA.

†Associate Professor, Department of Aerospace Engineering; currently retired.

for strake or forebody vortices to increase the lift on wing or body. Nowadays fighters making use of these vortices encounter problems with limit-cycle oscillations accompanied by large side forces (F-16), cyclic tail loads (F-18 and F-15), and recently a wing drop problem with the F-18E. Obviously the thorough knowledge of the features of such flows is important to make proper decisions during the design process to achieve the required aerodynamic properties.

In the crossflow field obtained by the slender-body approximation, the free vortex filaments near the contour will, except in some equilibrium positions as shown by de Laat and Coene,[5] have a certain velocity, which results in a rate of change of impulse in the two-dimensional crossflow field and thus a force on the contour. It is assumed that the body is in the center of a fixed coordinate system and that the body does not move in the cross plane.

In the first section the force acting on a two-dimensional circular cylinder by a symmetric vortex pair in oncoming flow is discussed. This force was first calculated by Bickley[6] using potential flow functions. Sarpkaya[7] calculated this force using an extended version of Lagally's theorem, which was faster to obtain because one did not have to go through the laborious integration of the unsteady pressure equations. In the next section the same force is even more simply obtained using conformal mapping and the generalized theorem of Routh.[8] The expression obtained is subsequently applied to a class of simple wing-body configurations. Zero-force curves, positive and negative-force areas, and maximum and minimum values of these flowfields are plotted and evaluated.

Furthermore, expressions are derived for wing-body contours in flows with nonsymmetrically disposed vortices that can arise either as a result of disturbances in the flow or by roll or sideslip of the aircraft.

In the last section the pressure distributions on the contour are decomposed in the $\frac{1}{2}\rho v \cdot v$ and $\rho \partial\phi/\partial t$ parts of the unsteady Bernoulli pressure equation to illustrate the contributions of both parts. Especially the contribution of the $\rho \partial\phi/\partial t$ part is interesting, as it is often omitted and yet it is an essential part in flowfields with free vortices.

II. Force on Circular Cylinder in Uniform Flow with Symmetric Free Vortex Pair

We consider the inviscid flowfield as described in Fig. 1. Because of the symmetry, there is only a force on the circle parallel to the x axis. This force is calculated by integration of the unsteady pressure at the circle, which was first reported by Bickley[6] and Tomotika and Sugawara.[9] The force can be written as

$$F_x = \frac{\rho\Gamma^2}{\pi}\frac{a^2}{r_1^3}\cos\theta_1\left[\frac{4r_1^2\sin^2\theta_1 - \left(r_1 - a^2/r_1\right)^2}{4a^2\sin^2\theta_1 + \left(r_1 - a^2/r_1\right)^2}\right] \tag{1}$$

where Γ is the absolute value of the strength of the vortices, which have equal strengths but different signs. This expression for the force generated by the symmetric vortex pair includes the $\rho \partial\phi/\partial t$ part of the pressure equation, which occurs in nonequilibrium positions. This expression is of practical use because only the position and strength of the vortices are required. The vortex velocities, which are more difficult to measure or estimate, are not required to be known. These vortex velocities are still present in Sarpkaya's[7] expression of this same force as an extension of Lagally's theorem. Calculating the vortex velocities using the Helmholtz theorem and the potential flow functions and substituting them in Sarpkaya's[7] equation for the drag again yields Eq. (1). Because of the symmetry of the vortex

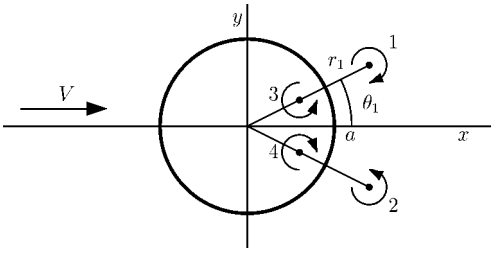

Fig. 1 Symmetric vortex pair behind a circle in uniform oncoming flow.

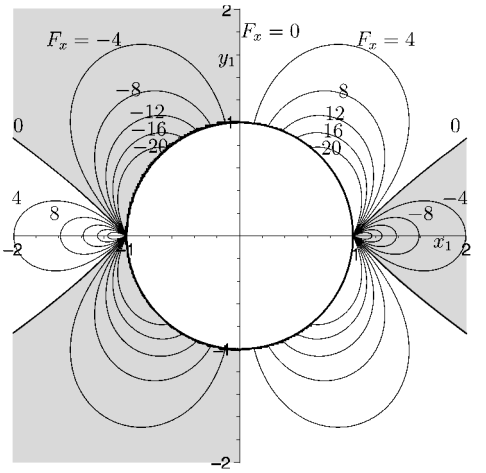

Fig. 2 Contour plot of the force F_x on the cylinder with the flowfield of Fig. 1 as a function of the position of vortex 1 (x_1, y_1) with $\rho = 1$, $\Gamma = 10$, and $a = 1$ [from Eq. (3): $F_{x_{max}} = 100/\pi$].

pairs in relation to V, the force is not dependent on V. A contour plot of the force as a function of the position of vortex 1 is given in Fig. 2. Bickley[6] stated that the resultant force is zero when the flowfield is stationary. This conclusion is right but not complete. We note from Eq. (1) that the force is zero for $\cos\theta_1 = 0$ or for

$$\pm 2\sin\theta_1 = 1 - a^2/r_1^2 \tag{2}$$

which are exactly the equations for the curves on which Föppl's equilibrium points are situated (e.g., Refs. 10 and 11). When the vortex pair is situated on these curves, however, the force on the circle is zero without imposing the extra condition $\Gamma/V = 2\pi r_1(1 - a^2/r_1^2)^2(1 + a^2/r_1^2)$ for zero vortex velocity, which yields the equilibrium points on the curves (2).

It is clear that in the equilibrium cases (for certain Γ/V) the flow will exert no force on the cylinder by virtue of d'Alembert's paradox as in these cases we have a two-dimensional inviscid stationary flowfield. It is new, however, that there is no force on the contour when the vortex pair is anywhere on the curves [Eq. (2)] independent of the value of Γ/V, so also when the vortices are moving and the flowfield is nonstationary. These zero-force curves are the curves at which the velocities of the mirror vortices, if they were free, would exactly be suited to continue fulfilling the boundary condition on the contour. So no forced motion of the mirror vortices, which ultimately is the "cause" of the force on the contour, is required to continue meeting the boundary condition. The zero-force curves are an interesting feature of this flowfield. Furthermore, if θ_1 is in the first quadrant of Fig. 2 it is also obvious from Eq. (1), as the other variables are positive, that F_x is positive (in the x direction) when the vortex pair is outside the zero-force curve, which means drag. When being between the zero-force curves, the vortex pair exerts a negative force F_x on the cylinder, which means thrust in relation to the direction of V. The negative force areas are shown in gray in Fig. 2. The maximum or minimum values at the circle are obtained from Eq. (1):

$$\lim_{r_1 \to a} F_x = (\rho\Gamma^2/\pi a)\cos\theta_1, \qquad \lim_{r_1 \to a} F_x(\theta_1 = 0) = -(\rho\Gamma^2/\pi a) \tag{3}$$

This extreme was given in Roy,[12] however, with an erroneous extra factor 2. The force has a maximum and a minimum value at $\theta_1 = 0$. The absolute value equals $F_{x_{max}} = \rho\Gamma^2/\pi a$. For a certain Γ the maximum force thus increases when decreasing the radius a of the circle. Furthermore, for $a \to \infty$ the cylinder effectively behaves as an infinite straight wall as discussed in the Appendix, and the force tends to zero.

The slender-body approximation of a circular aircraft forebody or circular missile at an angle of attack with vortices also yields this two-dimensional crossflow. When a vortex pair is intended to create a lift force, the vortex pair must be planned to be outside the zero-force curve as closely as possible to the maximum. If the vortex

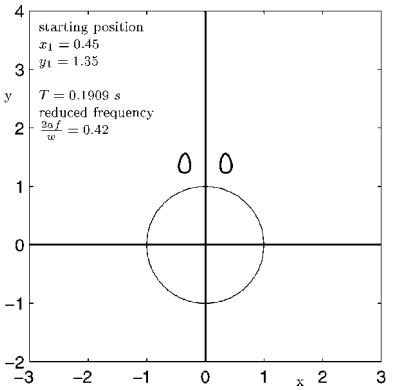

a) Trajectory of a symmetric vortex pair above a circle in upwash (from Ref. 5)

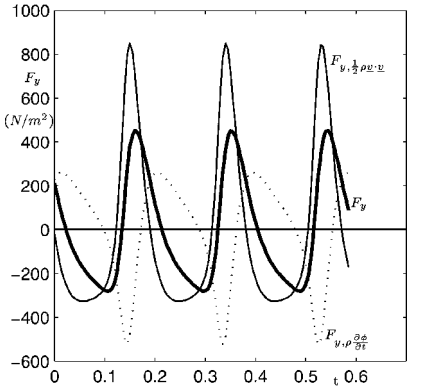

b) Force on the circle during the trajectory of Fig. 3a

Fig. 3 Trajectory of a symmetric vortex pair round its equilibrium position for $\Gamma = 80$ N/m^2, $w = 25$ m/s, and the force on the circle (with $a = 1$) during three cycles of the vortex trajectory with $\rho = 1$ kg/m^3.

pair were inside the zero-force curve, this would result in a negative vortex lift, which is generally not desired. In the two-dimensional case of a vortex pair behind a cylinder, it would be interesting to keep the vortex pair within the zero-force line. It would then yield a propulsive force. One might speculate on the well-known lowering of the pressure drag on a cylinder at a Reynolds number when a certain amount of vorticity is present in the wake of the cylinder within the zero-force curve.

To get an impression of the magnitude of the vortex force, this force is calculated during a symmetric motion of the vortex pair near the equilibrium positions[5] as shown in Fig. 3a, which is rotated 90 deg with respect to Fig. 1, so we have an upward flow with the vortices above the circle. The right-hand trajectory of course represents a counterclockwise motion, whereas the left-hand trajectory is clockwise. As a result of the symmetry, there is only a force in y direction. The force, displayed in Fig. 3b, was calculated with Eq. (1). As the picture is rotated 90 deg, the force is now called F_y. The contributions of the $\frac{1}{2}\rho \boldsymbol{v}\cdot\boldsymbol{v}$ and $\rho\partial\phi/\partial t$ parts of the unsteady pressure equation are both in Eq. (1) and are plotted separately in Fig. 3b to demonstrate their contributions. The time average of the force over one period is zero, as it should be. Furthermore the positions at which the force yields zero obviously are the points in time when the vortex pair crosses the zero-force curves. In dimensionless coefficients we have $c_{F_y} = F_y/\frac{1}{2}\rho w^2 2a$. For the maximum value of F_y in this example, this yields $c_{F_y} \approx 0.7$.

III. Force of Symmetric Vortex Pair Behind Symmetric Contour, Using Conformal Mapping

The calculation of the force [Eq. (1)] was done by carrying out the laborious unsteady pressure integration, which was reported by Bickley[6] and Tomotika and Sugawara.[9] Using Sarpkaya's[7] extension of Lagally's theorem and Helmholtz's theorem to calculate the vortex velocities, it was easier to derive Eq. (1). We note that Eq. (1) is valid for a circular contour only. It will be shown that the force as a function of vortex strength and position on a more general symmetric contour can be obtained more simply by a general conformal mapping with real coefficients, implying $\zeta(z) = \zeta(\bar{z})$. First the simple case of the Joukowski transformation (Fig. 4) is considered.

The flowfield in the ζ plane is a uniform flow with a symmetric vortex pair, in which a flat plate parallel to the flow does not disturb the flow. This flow can be simply described. We will use the flowfield in the ζ plane as starting point to describe the flowfield in the z plane by conformal transformation. It is clear that the force on a contour equals the rate of change of the impulse in the flowfield. For this symmetric case the impulse of the vortex pair in the ζ plane equals $2\rho\Gamma Im(\zeta_1)$ (Ref. 13), and because of the symmetry there is only a force in ξ direction, which equals the rate of change of impulse:

$$F_\xi = 2\rho\Gamma Im\left(\frac{\mathrm{d}\zeta_1}{\mathrm{d}t}\right)$$

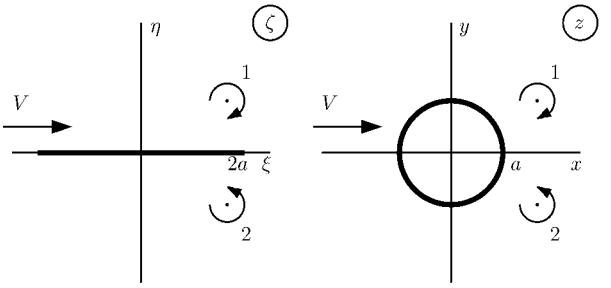

Fig. 4 Joukowski transformation ($\zeta = z + a^2/z$) of a symmetric vortex pair in a uniform flow to a symmetric vortex pair behind a circle in uniform flow ($\zeta = \xi + \eta i$ and $z = x + yi$).

To calculate the force on the contour in the z plane, we will now use $\zeta = \zeta(z)$, and so

$$F_x = 2\rho\Gamma Im\left(\frac{\mathrm{d}\zeta_1}{\mathrm{d}z_1}\frac{\mathrm{d}z_1}{\mathrm{d}t}\right) \tag{4}$$

The vortex velocity in the z plane $(\mathrm{d}z_1/\mathrm{d}t)$ is related to the vortex velocity in the ζ plane. However, the vortex velocity does not simply transform with the conformal mapping. It changes according to the change of path function described by the generalized theorem of Routh.[8] Hence the force on the contour from the vortices consequently changes by the transformation. With $(\mathrm{d}\zeta/\mathrm{d}z)_{z=z1} = \zeta_1'$ and $(\mathrm{d}^2\zeta/\mathrm{d}z^2)_{z=z1} = \zeta_1''$ we have

$$\overline{\frac{\mathrm{d}z_1}{\mathrm{d}t}} = u_1 - v_1 i = \left(\frac{\mathrm{d}\chi}{\mathrm{d}\zeta} - \frac{\Gamma i}{2\pi}\frac{1}{\zeta - \zeta_1}\right)_{\zeta=\zeta_1}\zeta_1' + \frac{\Gamma i}{4\pi}\left(\frac{\zeta_1''}{\zeta_1'}\right) \tag{5}$$

Substitution of Eq. (5) into Eq. (4) and using $\mathrm{d}\zeta_1/\mathrm{d}z_1 = (\mathrm{d}\zeta/\mathrm{d}z)_{z=z1}$ yields

$$F_x = 2\rho\Gamma Im\left[\left(\overline{\frac{\mathrm{d}\chi}{\mathrm{d}\zeta} - \frac{\Gamma i}{2\pi}\frac{1}{\zeta - \zeta_1}}\right)_{\zeta=\zeta_1}|\zeta_1'|^2\right] - \frac{\rho\Gamma^2}{2\pi}Re\left(\overline{\frac{\zeta_1''}{\zeta_1'}}\zeta_1'\right)$$

The first part is proportional to the imaginary part of the conjugate vortex velocity in the ζ plane, which equals zero, and so

$$F_x = -\frac{\rho\Gamma^2}{2\pi}Re\left(\overline{\frac{\zeta_1''}{\zeta_1'}}\zeta_1'\right) \tag{6}$$

Now we have an expression for the force on the contour as a result of the symmetric vortex pair using only the derivatives of the transformation, applied on the vortex position. Compliance with the boundary condition on the contour is ensured by the conformal mapping.

Substitution of the Joukowski transformation $\zeta = z + a^2/z$ (Fig. 4), which yields the contour of a circle with radius a in the z plane, yields after some simplification

$$F_x = -\frac{\rho\Gamma^2}{\pi}\frac{a^2}{r_1^2} Re\left[\frac{z_1^2 - a^2}{z_1\left(\overline{z_1}^2 - a^2\right)}\right] \tag{7}$$

with $r_1 = |z_1|$. Substitution of $z_1 = r_1 e^{i\theta_1}$ yields Eq. (1), and we have again the unsteady force (including $\rho\partial\phi/\partial t$ term) of a (moving) symmetric vortex pair behind a circle with oncoming flow, as a function of the vortex position.

Any symmetric conformal transformation with real coefficients, which keeps the vortices symmetric and outside the contour, can be substituted into Eq. (6). Hence we have a result with which we can calculate the force on a transformed symmetric contour as a function of the first- and second-order derivatives of the mapping function at the vortex position. Force calculations using this expression are straightforward when vortex strengths and positions are known. The expression can be used in aeronautical applications, in which mainly symmetric contours are applied, and with conformal mapping all kinds of contours can be obtained. In the next section this expression is applied for a symmetric vortex pair above a simple wing-body combination.

IV. Force on Wing-Body Combination with Symmetric Free Vortex Pair in Upwash

We adapt Eq. (6) for a vortex pair with a vertical impulse:

$$F_y = -(\rho\Gamma^2/2\pi)Im[(\overline{\zeta_1''}/\overline{\zeta_1'})\zeta_1'] \tag{8}$$

To obtain the flowfield of the vortex pair over a wing-body configuration in upflow, we apply a transformation (Fig. 5) as follows:

$$\zeta = \sqrt{(\zeta^*)^2 - 4a^2}$$

(Brown and Michael[14]), $\zeta^* = z + c^2/z$. Elimination of ζ^* yields

$$\zeta = \sqrt{(z + c^2/z)^2 - 4a^2} \tag{9}$$

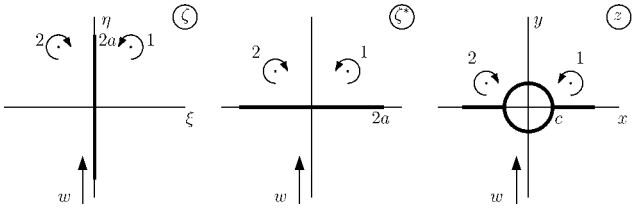

Fig. 5 Conformal mapping for application of Eq. (8) on a simple wing-body combination in symmetric flow.

Substitution of Eq. (9) into Eq. (8) yields the force of the flowfield of the symmetric vortex pair with upwash w on the wing-body combination:

$$F_y = -\frac{\rho\Gamma^2}{2\pi} Im\left\{\left[\frac{1 + 3\left(c^4/z_1^4\right)}{z_1 - \left(c^4/z_1^3\right)} - \frac{z_1 - c^4/z_1^3}{\left(z_1 + c^2/z_1\right)^2 - 4a^2}\right] \times \frac{z_1 - c^4/z_1^3}{\sqrt{\left(z_1 + c^2/z_1\right)^2 - 4a^2}}\right\} \tag{10}$$

Of course, only position and strength of the vortices are required. Because of the symmetry, the force is independent of w.

In Fig. 6 the force F_y is plotted as a function of the vortex position (x_1, y_1) for three values of wingspan $s = 2[a + \sqrt{(a^2 - c^2)}]$ by changing a. The case with $c = 1$ and $a = 2$ is also treated in de Laat and Coene[5] for the equilibrium and motion of the vortices. Comparing this figure with the curve of equilibrium points given there, we note that the curves on which the equilibrium points are located are identical to the plotted zero-force curves, which yield zero force independent of Γ/w. For these wing-body configurations there are also negative force areas, which are indicated in gray in Fig. 6. The maximum and minimum values for F_y at $(x_1 = c, y_1 = 0)$ are

$$\lim_{x_1 \to c} F_y(y_1 = 0) = +\frac{\rho\Gamma^2}{\pi\sqrt{a^2 - c^2}}$$

$$\lim_{y_1 \to 0} F_y(x_1 = c) = -\frac{\rho\Gamma^2}{\pi\sqrt{a^2 - c^2}}$$

and at $(x_1 = 0, y_1 = c)$ we have

$$\lim_{y_1 \to c} F_y(x_1 = 0) = -\rho\Gamma^2/\pi a, \qquad \lim_{x_1 \to 0} F_y(y_1 = c) = +\rho\Gamma^2/\pi a$$

Thus, when the span $\{s = 2[a + \sqrt{(a^2 - c^2)}]\}$ is increased (increasing a or decreasing c) the maximum force decreases. This is analogous to the case of the circle in which the force decreased with increasing radius. When the span goes to infinity, the flowfield of a vortex near an infinite wall (as in the Appendix) is approximated, and the force will go to zero. We can conclude that the force induced by vortices on a contour will generally decrease when enlarging the width of the contour perpendicular to the direction of that force. This is relevant to the effect of vortices, which are intended to contribute to the lift force of an aircraft. It means that a vortex with a certain strength above a wing or body and parallel to the aircraft longitudinal axis in a slender-body approximation in crossflow produces more lift when the span or body width is reduced. The position of the vortex over the wing or body is delicate, however, as there are positions where the vortex force is negative and thus acts in the direction opposite to the lift force.

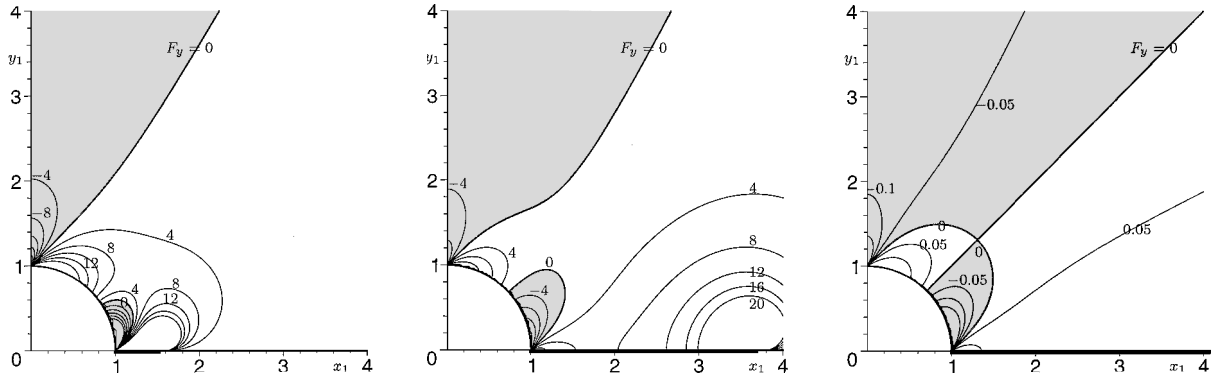

Fig. 6 Force F_y as a function of the vortex position (x_1, y_1) for the flowfield of Fig. 5 in the z plane for $\rho = 1$ and $\Gamma = 10$ with $c = 1$ and, respectively, $a = 1.1$, $a = 2$, and $a = 100$.

V. Force on Wing-Body Combination by a (Not Necessarily Symmetric) Vortex Pair

An asymmetric vortex pair above a wing-body configuration arises from the slender-body approximation of an aeroplane with asymmetric vortices over the wing coming from the forebody, strakes, or canard surfaces, at an angle of attack with a uniform velocity. These flowfields were studied by Sacks[15] and Sacks et al.,[16] however, without evaluating the $\rho\partial\phi/\partial t$ part. To investigate these flows, we use conformal mapping to transform the circle into a simple wing-body combination (Fig. 7) by combining two transformations as follows:

$$\zeta^* = \zeta + a^2/\zeta, \qquad \zeta^* = z + c^2/z$$

Elimination of ζ^* and expressing ζ in z yields

$$\zeta = \tfrac{1}{2}\left[z + c^2/z + \sqrt{(z + c^2/z)^2 - 4a^2}\right] \tag{11}$$

The force exerted on a stationary body by an unsteady flow is calculated with the unsteady version of Blasius's theorem[10]:

$$F_x + iF_y = \overline{\frac{i\rho}{2}\int\left(\frac{\mathrm{d}\chi}{\mathrm{d}z}\right)^2 \mathrm{d}z} - i\rho\frac{\partial}{\partial t}\int \chi\,\mathrm{d}z \tag{12}$$

The $\frac{1}{2}\rho\boldsymbol{v}\cdot\boldsymbol{v}$ and $\rho\partial\phi/\partial t$ parts of Eq. (12) will now be evaluated separately. Because the force caused by the $\frac{1}{2}\rho\boldsymbol{v}\cdot\boldsymbol{v}$ part follows from the velocities of the free outer vortices as shown by Sarpkaya,[7] extending Lagally's theorem, we have

$$F_{x,\frac{1}{2}\rho\boldsymbol{v}\cdot\boldsymbol{v}} + iF_{y,\frac{1}{2}\rho\boldsymbol{v}\cdot\boldsymbol{v}} = \overline{\frac{i\rho}{2}\int\left(\frac{\mathrm{d}\chi}{\mathrm{d}z}\right)^2\frac{\mathrm{d}\zeta}{\mathrm{d}z}\,\mathrm{d}\zeta} = i\rho(\Gamma_2\dot{z}_2 - \Gamma_1\dot{z}_1) \tag{13}$$

The $\rho\partial\phi/\partial t$ pressure part

$$F_{x,\rho\partial\phi/\partial t} + iF_{y,\rho\partial\phi/\partial t} = -i\rho\frac{\partial}{\partial t}\left([\chi z]_{\text{contour}} + \int z\frac{\mathrm{d}\chi}{\mathrm{d}z}\,\mathrm{d}z\right) \tag{14}$$

has to be calculated, however. The first term on the right-hand side of Eq. (14) equals zero as the potential is continuous on the contour. Rewriting Eq. (14) for integration in the ζ plane, substituting the inverse of transformation (11) and the potential flow function (χ) of the flowfield around the circle (ζ plane in Fig. 7)

$$\chi(\zeta;\zeta_1,\zeta_2) = \frac{\Gamma_1 i}{2\pi}\ln\left(\frac{\zeta - a^2/\overline{\zeta_1}}{\zeta - \zeta_1}\right) + \frac{\Gamma_2 i}{2\pi}\ln\left(\frac{\zeta - \zeta_2}{\zeta - a^2/\overline{\zeta_2}}\right) - wi\left(\zeta - \frac{a^2}{\zeta}\right) \tag{15}$$

and subsequently evaluating the residues of the singularities inside the circle to calculate the integrals, we obtain

$$F_{x,\rho\partial\phi/\partial t} + iF_{y,\rho\partial\phi/\partial t} = -\rho\Gamma_1 i\frac{\partial}{\partial t}\left[\frac{a^2}{\zeta_1} + \frac{1}{2}\frac{a^2}{\overline{\zeta_1}} - \frac{1}{2}\overline{\zeta_1} + \sqrt{\left(\frac{a^2}{\overline{\zeta_1}} + \overline{\zeta_1}\right)^2 - 4c^2}\right] + \rho\Gamma_2 i\frac{\partial}{\partial t}\left[\frac{a^2}{\zeta_2} + \frac{1}{2}\frac{a^2}{\overline{\zeta_2}} - \frac{1}{2}\overline{\zeta_2} + \sqrt{\left(\frac{a^2}{\overline{\zeta_2}} + \overline{\zeta_2}\right)^2 - 4c^2}\right]$$

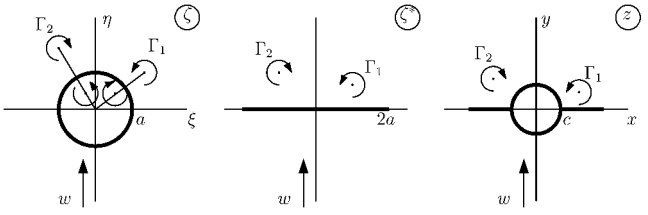

Fig. 7 Transformation of the nonsymmetric flowfield round a circle to the flowfield of a wing-body combination.

Substitution of $c = 0$ yields the $\rho\partial\phi/\partial$t part of the force on the flat plate derived by Sarpkaya.[17] Substitution of the transformation (11) and execution of the differentiations yields for the force from integration of the $\rho\partial\phi/\partial t$ part of the pressure:

$$F_{x,\rho\partial\phi/\partial t} + iF_{y,\rho\partial\phi/\partial t} = \rho\Gamma_1 i\left[\frac{a^2}{\zeta_1^2}\frac{\mathrm{d}\zeta_1}{\mathrm{d}z_1}\dot{z}_1 - \left(1 - \frac{\mathrm{d}\bar{\zeta}_1}{\mathrm{d}\bar{z}_1}\right)\dot{\bar{z}}_1\right] - \rho\Gamma_2 i\left[\frac{a^2}{\zeta_2^2}\frac{\mathrm{d}\zeta_2}{\mathrm{d}z_2}\dot{z}_2 - \left(1 - \frac{\mathrm{d}\bar{\zeta}_2}{\mathrm{d}\bar{z}_2}\right)\dot{\bar{z}}_2\right] \tag{16}$$

Addition of the $\frac{1}{2}\rho\boldsymbol{v}\cdot\boldsymbol{v}$ part (13) and $\rho\partial\phi/\partial t$ part (16) of the pressure integral yields for the total force:

$$F_x + iF_y = -\rho\Gamma_1 i\left[\left(1 - \frac{a^2}{\zeta_1^2}\frac{\mathrm{d}\zeta_1}{\mathrm{d}z_1}\right)\dot{z}_1 + \left(1 - \frac{\mathrm{d}\bar{\zeta}_1}{\mathrm{d}\bar{z}_1}\right)\dot{\bar{z}}_1\right] + \rho\Gamma_2 i\left[\left(1 - \frac{a^2}{\zeta_2^2}\frac{\mathrm{d}\zeta_2}{\mathrm{d}z_2}\right)\dot{z}_2 + \left(1 - \frac{\mathrm{d}\bar{\zeta}_2}{\mathrm{d}\bar{z}_2}\right)\dot{\bar{z}}_2\right] \tag{17}$$

The vortex velocities are easily determined with the potential flow function and transformation using the generalized theorem of Routh.[8] The force [Eq. (17)] during the motion of a vortex around its equilibrium position is plotted in Fig. 8. Vortex 2 is very near its equilibrium position. Vortex 1 is displaced from its equilibrium position and therefore describes a nearly periodic trajectory, counterclockwise as described in de Laat and Coene.[5] For symmetric cases not shown here, the forces calculated with Eq. (10) obviously are the same as those of Eq. (17). We would like to point out that in Fig. 8b the side force is larger than the lift force. This is clearly related to the width of the contour perpendicular to x (height) being smaller than the width perpendicular to y (span). In Figs. 8c and 8d the side force and lift force are shown together with the separate contributions of the $\frac{1}{2}\rho\boldsymbol{v}\cdot\boldsymbol{v}$ and $\rho\partial\phi/\partial t$ parts to the resulting total force. These examples demonstrate the importance of the $\rho\partial\phi/\partial t$ contribution to the pressure force on a contour in flows with vortices.

VI. Pressure Distribution

To get a better understanding of the force on the contour, we will now investigate the pressure distributions for the cases of the vortex pair positioned behind a circle in uniform flow and the vortex pair above the simple wing-body combination. Therefore the spanwise contributions of the $\frac{1}{2}\rho\boldsymbol{v}\cdot\boldsymbol{v}$ and $\rho\partial\phi/\partial t$ part of the unsteady pressure will be evaluated. In the Appendix the pressure distribution on a straight infinite wall of the flowfield of a single vortex and a uniform parallel flow along that wall is given. We see there that there is a certain resultant pressure distribution, which is independent of V and that the integral of the pressure on the wall equals zero, so that there is no resultant force on the wall. For the finite contours treated here we know from the preceding sections that the forces for the symmetric flowfields are independent of the strength of the uniform flow (V or w). The pressure distributions, however, will be shown to vary.

A. Pressure Distribution for the Symmetric Vortex Pair Near the Circle

To investigate the pressure distribution, a computer plot of the pressure on the circle of the flowfield of the vortex pair near the circle, described in the first section but rotated over 90 deg, will be made. The complex potential flow function at the contour will be used to calculate the $\frac{1}{2}\rho\boldsymbol{v}\cdot\boldsymbol{v}$ part. As on the contour, the streamfunction ψ equals zero; the $\partial\phi/\partial t$ part can be replaced by $\partial\chi/\partial t$. The rate of change of the potential function is caused by the displacement of the vortices, and so we have

$$\frac{\partial\phi}{\partial t} = \frac{\partial\chi}{\partial t} = \frac{\partial\chi}{\partial z_1}\frac{\partial z_1}{\partial t} + \frac{\partial\chi}{\partial\bar{z}_1}\frac{\partial\bar{z}_1}{\partial t} \tag{18}$$

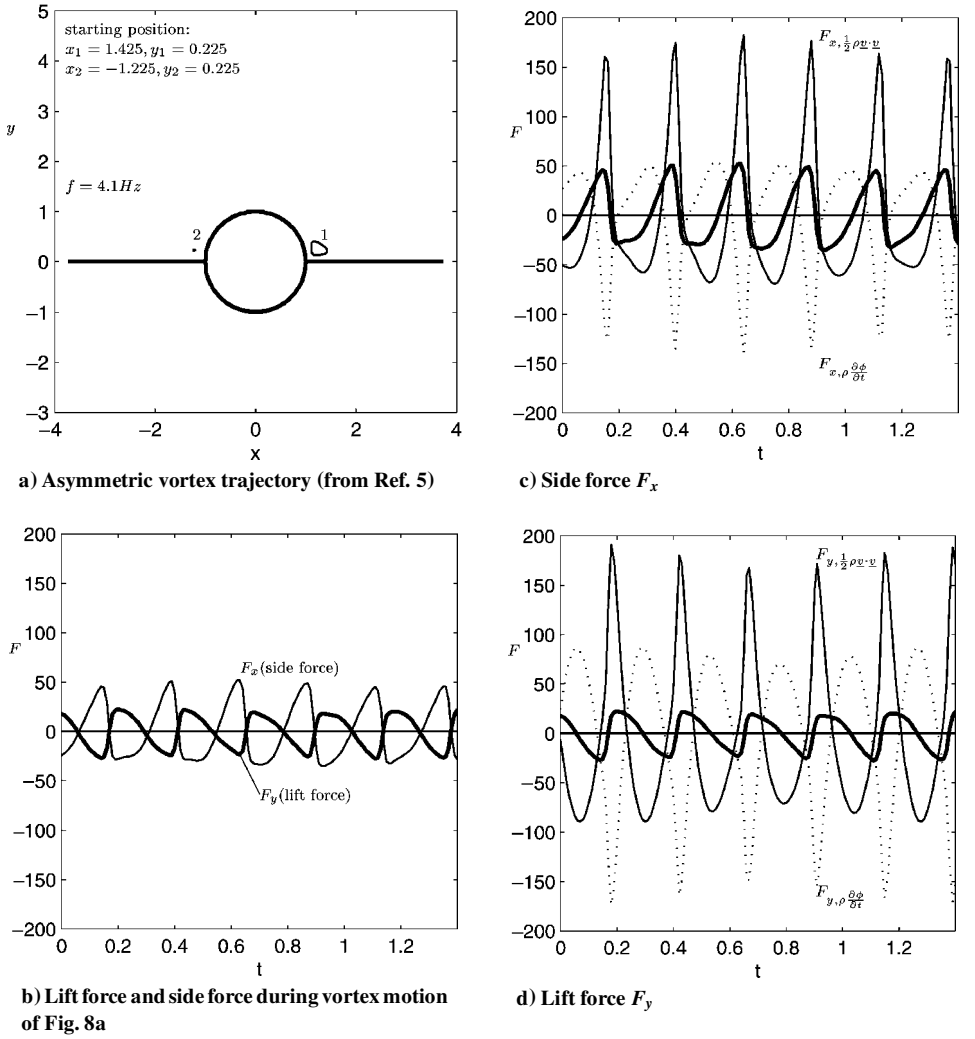

a) Asymmetric vortex trajectory (from Ref. 5)

c) Side force F_x

b) Lift force and side force during vortex motion of Fig. 8a

d) Lift force F_y

Fig. 8 Asymmetric vortex trajectory of a vortex pair above a wing-body combination and the lift and side forces during the vortex motion for $a = 2$, $c = 1$, $w = 25$, $\Gamma_1 = \Gamma_2 = 25$, and $\rho = 1$.

The required vortex velocity $\mathrm{d}z_1/\mathrm{d}t = u_1 + v_1 i$ is obtained with Helmholtz's theorem, using the complex conjugate of $\mathrm{d}\chi/\mathrm{d}z$. Substitution of the vortex velocity and the derivatives $\partial\chi/\partial z_1$ and $\partial\chi/\partial\bar{z}_1$ into Eq. (18) yields the $\rho\partial\phi/\partial t$ part of the pressure on the contour.

In Fig. 9a the pressure difference between the upper and lower side caused by the vortex pair in its equilibrium is plotted. Because the vortices are accurately placed in their equilibrium positions, their velocity is zero, and the flowfield is stationary; thus, there is no contribution to the pressure distribution from the $\rho\partial\phi/\partial t$ part. The $\frac{1}{2}\rho v\cdot v$ part does give a pressure distribution, as can be seen in Fig. 9a. Numerical integration of this pressure distribution yields zero, which is in accordance with d'Alembert's paradox and Eq. (1). In Figs. 9b and 9c the flowfields are plotted with the same parameters as Fig. 9a, but now for cases in which the vortices are not in their equilibrium positions but slightly displaced to respectively the negative and positive side of the zero-force curve (see Fig. 2). In these cases there is a contribution of the $\rho\partial\phi/\partial t$ part. In Fig. 9b it counteracts the $\frac{1}{2}\rho v\cdot v$ part, and in Fig. 9c it works in the same direction. In Fig. 9d the same vortex configuration is shown as in Fig. 9c but now when there is no upwash ($w = 0$). The pressure distributions are quite different, but the resulting force is the same, which we already knew from Eq. (1). When w equals zero, the $\rho\partial\phi/\partial t$ part, and the $\frac{1}{2}\rho v\cdot v$ part of the pressure equation has opposite signs everywhere on the surface. The two parts of the pressure equation counteract. When the radius of the circle tends to infinity, we have again the vortices near an infinite straight wall as in the Appendix, and the force tends to zero.

B. Pressure Distribution for the Vortex Pair Above the Wing-Body Combination

The pressure distribution on the contour of the wing-body combination (Fig. 7) is investigated in the same way as the circle, by separately calculating the contributions of $\frac{1}{2}\rho v\cdot v$ and $\rho\partial\phi/\partial t$. The $\frac{1}{2}\rho v\cdot v$ part is determined from the potential flow function (15) and transformation (11) by $u - vi = (\partial\chi/\mathrm{d}\zeta)(\mathrm{d}\zeta/\mathrm{d}z)$. For the $\rho\partial\phi/\partial t$ part we again use the fact that at the contour the streamfunction ψ equals zero, and thus $\partial\chi/\partial t = \partial\phi/\partial t$. The partial differentiation now has the form

$$\frac{\partial\chi}{\partial t} = \frac{\partial\chi}{\partial\zeta_1}\frac{\mathrm{d}\zeta_1}{\mathrm{d}z_1}\frac{\partial z_1}{\partial t} + \frac{\partial\chi}{\partial\bar{\zeta}_1}\frac{\mathrm{d}\bar{\zeta}_1}{\mathrm{d}\bar{z}_1}\frac{\partial\bar{z}_1}{\partial t} + \frac{\partial\chi}{\partial\zeta_2}\frac{\mathrm{d}\zeta_2}{\mathrm{d}z_2}\frac{\partial z_2}{\partial t} + \frac{\partial\chi}{\partial\bar{\zeta}_2}\frac{\mathrm{d}\bar{\zeta}_2}{\mathrm{d}\bar{z}_2}\frac{\partial\bar{z}_2}{\partial t} \tag{19}$$

The vortex velocities ($\mathrm{d}z_1/\mathrm{d}t$, $\mathrm{d}\bar{z}_1/\mathrm{d}t$, $\mathrm{d}z_2/\mathrm{d}t$, $\mathrm{d}\bar{z}_2/\mathrm{d}t$) are calculated with Eq. (5) using the equations in the ζ plane and the transformation. Substitution of the derivatives of Eqs. (15) and (11) and the vortex velocities into Eq. (19) yields the $\rho\partial\phi/\partial t$ contribution to the surface pressure.

In Fig. 10 the pressure differences between upper and lower side are plotted for three values of w at a certain $\Gamma = \Gamma_1 = -\Gamma_2$. The vortices are positioned in an arbitrary place above the wing. The $\frac{1}{2}\rho v\cdot v$ and $\rho\partial\phi/\partial t$ contributions are shown separately to demonstrate that at a large value of w the $\frac{1}{2}\rho v\cdot v$ contribution is negative but that the $\rho\partial\phi/\partial t$ in this example is positive. At low values of w, the opposite is the case. In this symmetrical flow the resulting force is

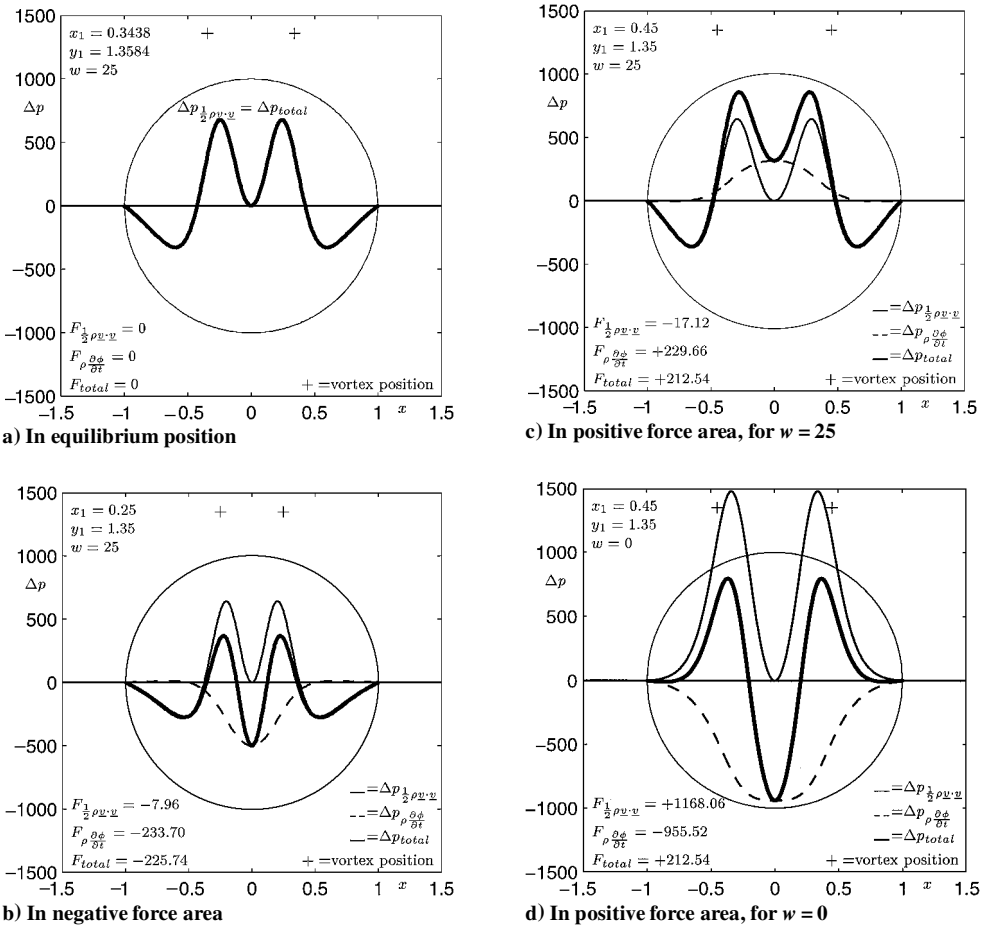

Fig. 9 Pressure difference between upper and lower side for $a = 1$, $\rho = 1$, $\Gamma = 80$ with the vortices in their equilibrium positions, in the negative force area and positive force area for $w = 25$ and $w = 0$.

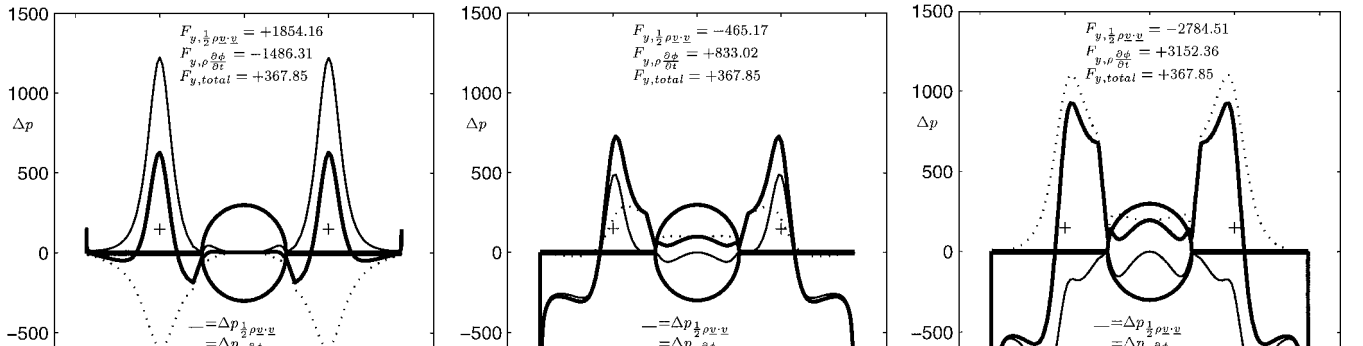

Fig. 10 Pressure difference between upper and lower side of a wing-body configuration with a symmetric vortex pair, for $a = 2$, $c = 1$, $\rho = 1$, $\Gamma_1 = -\Gamma_2 = 80$, $x_1 = 2.0$, $y_1 = 0.5$, $x_2 = -2.0$, $y_2 = 0.5$, and, respectively, $w = 0$, 25, and 50.

independent of the value of w, as was already known from Eq. (10), but the pressure distributions vary substantially for different values of w. In the limit with a tending to infinity and c equaling zero (span tends to infinity), the total force will tend to zero as is the case with the vortex near the infinite straight wall in the Appendix.

In Fig. 11 separate pressure distributions on upper and lower surfaces are plotted for the same wing-body combination as in Fig. 10. In this example the vortices are put near the wing tips, and we imagine that this wing-body combination is the result of a slender-body approximation of a delta wing with body and that there are leading-edge vortices. Their strengths are calculated to fulfill the Kutta condition at the wing tip. The vortices are clearly in the positive force region of Fig. 6b, which has the same geometry ($a = 2$ and $c = 1$) as Figs. 10 and 11. The $\frac{1}{2}\rho v \cdot v$ part, $\rho \partial\phi/\partial t$ part, and total pressure distributions are plotted in separate figures to clearly show the contributions of both terms. The total pressure distribution of Fig. 11c shows the familiar picture for the pressure distribution of such a flowfield. In Figs. 11a and 11b we see that the peaks at the vortex position are from the $\frac{1}{2}\rho v \cdot v$ part and the flat pressure distribution in between is from the $\rho \partial\phi/\partial t$ part. In this case the $\frac{1}{2}\rho v \cdot v$ and $\rho \partial\phi/\partial t$ part work in the same direction instead of counteracting.

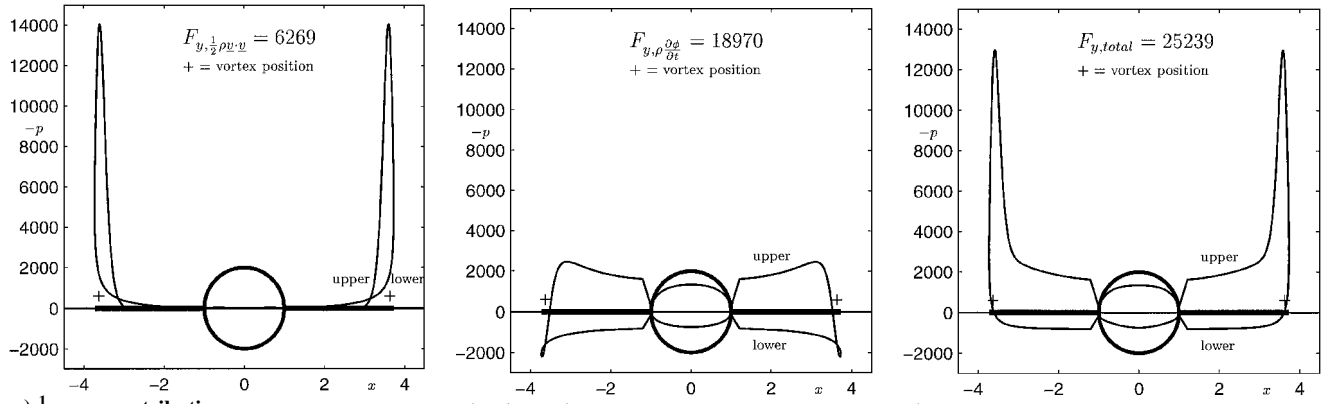

Fig. 11 The $\frac{1}{2}\rho v \cdot v$ and $\rho\partial\phi/\partial t$ parts of the pressure distributions on upper and lower surfaces for $a = 2$, $d = 1$, $\rho = 1$, $w = 25$, $\Gamma_1 = -\Gamma_2 = 211.77$, $x_1 = 3.63$, $y_1 = 0.3$, $x_2 = -3.63$, and $y_2 = 0.3$.

VII. Conclusions

Zero-force curves have been found for the vortex pair positioned behind a circular cylinder in oncoming flow or for the vortex pair above a wing-body combination in upwash. The zero-force curve behind the cylinder was found to be the same curve on which the Föppl equilibrium points are situated for specific values of Γ/V. The force, however, equals zero everywhere on the curve independent of Γ/V, even when the flow is nonstationary and when the vortices are crossing this curve. The force on the contour is in the downwind direction (vortex drag) when the vortex pair is positioned outside the zero-force curve in the first quadrant. Inside this zero-force curve the vortex pair exerts an upwind force F_x on the cylinder (vortex thrust). This phenomenon might in the viscous real world be related to the lowering in drag at a certain Reynolds number when enough vorticity is present within a certain area behind the cylinder.

An expression has been derived with which the force of a symmetric vortex pair on a symmetric contour, obtained by conformal mapping from a simple symmetric vortex pair, can directly be calculated with the first- and second-order derivatives of the mapping function. This expression has been applied to a simple class of wing-body combinations. Areas of negative lift force have been identified for these configurations, and the equilibrium curves are shown to be zero-force curves as well, independent of Γ/w, so also for nonstationary flows. The negative force areas are important when designing an aircraft with strakes or forebody vortices over body or wing areas intended to increase lift. When the vortices are situated within the negative force area, this leads to an undesired lowering of lift, which for example might be the explanation for the wing-drop problem with the F-18E. This problem was solved by influencing the strake vortices through blowing over the strakes. The knowledge in this paper might help planning the vortex position above the wing or body for optimum increased lift and preventing a loss of lift.

Furthermore, it has been found that the force induced by vortices on a contour will generally decrease when enlarging the width of the contour perpendicular to the direction of that force. This has a major consequence for the effect of vortices, which are intended to contribute to the lift force of an aircraft. It means that a vortex with a certain strength above a wing or body and parallel to the aircraft longitudinal axis in a slender-body approximation produces more lift when the span or body width is reduced. For aircraft encountering the tip vortex of another aircraft, the resulting force will be larger when the encountering aircraft has a smaller wing span.

Simple analytical expressions have been derived, using conformal mapping, for the force of a not necessarily symmetric vortex pair above a wing-body combination in a uniform upwash. For flowfields of aircraft with asymmetric vortices above wing or body, the side force that occurs will generally be larger than the vortex lift force. These large side forces are an explanation for the large yawing moments experienced with asymmetric forebody vortices near the surfaces of aircraft and missiles.

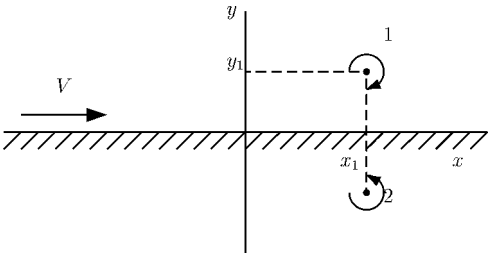

Fig. A1 Vortex near an infinite straight wall ($y = 0$).

Finally, it was found that the pressure distribution (and so the bending moment) on the contour as a result of a symmetric vortex pair varies with changing speed of the oncoming flow. The resulting force, however, does not vary and was found to be independent of the speed of the oncoming flow. The contributions of the $\frac{1}{2}\rho v \cdot v$ and $\rho\partial\phi/\partial t$ parts of the unsteady pressure to the force on the contour have been illustrated.

The preceding findings are for the unsteady, inviscid two-dimensional slender-body approximated flowfields. The areas with negative vortex lift, the reduced vortex lift with increasing wing span, and the large side forces for asymmetric vortex flows are important effects to be considered when designing an airplane. The knowledge of the reported unsteady inviscid features could help to understand the more complex measurements and calculations of the real three-dimensional unsteady viscous flow.

Appendix: Pressure and Force of a Single Vortex on an Infinite Straight Wall

We consider a vortex near an infinite wall as in Fig. A1. The potential flow function ϕ of a point (x, y) in the flowfield with vortex 1 at the coordinates (x_1, y_1) is described by

$$\phi = (\Gamma/2\pi)[\arctan(y - y_1)/(x - x_1) - \arctan(y + y_1)/(x - x_1)] + Vx \tag{A1}$$

The pressure on the wall is calculated with the unsteady Bernoulli equation:

$$p = \text{constant} - \frac{1}{2}\rho v \cdot v - \rho\frac{\partial\phi}{\partial t} \tag{A2}$$

On the wall ($y = 0$) we obtain with constant $= \frac{1}{2}\rho V^2$

$$p_{\frac{1}{2}\rho v\cdot v} = \text{constant} - \frac{1}{2}\rho v \cdot v = \frac{1}{2}\rho V^2 - \frac{\rho}{2}\left[\frac{\Gamma}{\pi}\frac{y_1}{(x - x_1)^2 + y_1^2} + V\right]^2 \tag{A3}$$

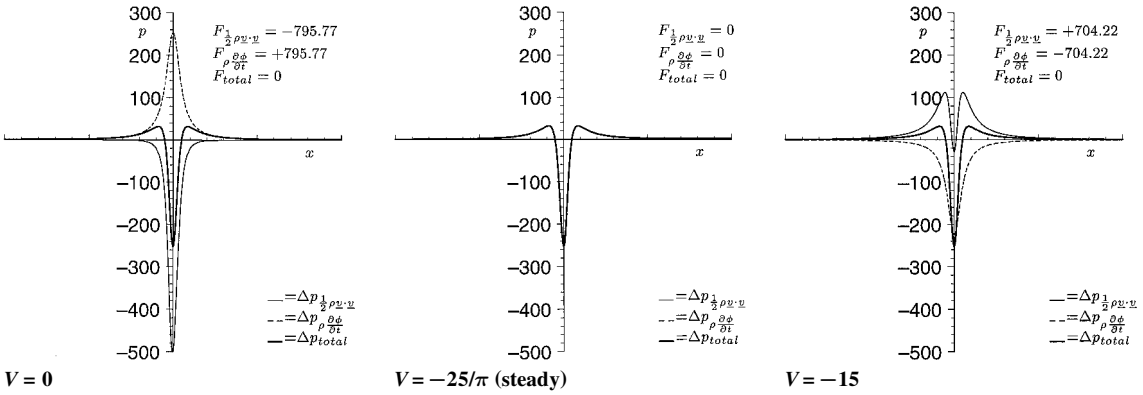

Fig. A2 Pressure distribution on an infinite straight wall from a vortex flow near that wall for $x_1 = 0$, $y_1 = 1$, $\rho = 1$, and $\Gamma = 100$ for three values of V.

The $\rho\partial\phi/\partial t$ part of the pressure equation is determined by the motion of the vortices, and so we put

$$\frac{\partial\phi}{\partial t} = \frac{\partial\phi}{\partial x_1}\frac{\mathrm{d}x_1}{\mathrm{d}t}$$

The vortex velocity $u_1 = \mathrm{d}x_1/\mathrm{d}t$ is calculated using the Helmholtz theorem with the flowfield velocity at its position. The $\partial\phi/\partial x_1$ factor is obtained from Eq. (A1) for $y = 0$ on the wall, which yields

$$p_{\rho\frac{\partial\phi}{\partial t}} = -\rho\frac{\partial\phi}{\partial t} = \frac{\rho\Gamma}{\pi}\frac{\Gamma/4\pi + Vy_1}{(x - x_1)^2 + y_1^2} \tag{A4}$$

In Fig. A2 the pressure distributions for three cases are plotted. The total force on the wall is obtained by integrating the pressure, which of course yields zero for all vortex positions. When altering the uniform speed V, the separate contributions of the $\frac{1}{2}\rho v\cdot v$ and $\rho\partial\phi/\partial t$ parts change. The resulting (total) pressure distribution on the wall, however, will not be changed. Obviously the pressure distribution is nonvarying under a Galilei transform with varying velocity V. This is not the case for the effect of vortices on the finite contours in the present paper, in which the total pressure distribution does change with V, although the total force remains independent of V.

References

[1]Skow, A. M., and Erickson, G. E., "Modern Fighter Aircraft Design for High Angle of Attack Manoeuvring," LS-121, Paper 4, AGARD, Dec. 1982.

[2]Cheng, H. K., Edwards, R. H., Jia, Z. X., and Lee, C. J., "Vortex Dominated Slender Wing Problems; Studies by a Point-Vortex Method," *Proceedings of the AIAA/ASME 1st National Fluid Dynamics Congress*, Pt. 1, AIAA, Washington, DC, 1998, pp. 512–522.

[3]Rossow, V. J., "Estimate of Loads During Wing-Vortex Interactions by Munk's Transverse-Flow Method," *Journal of Aircraft*, Vol. 27, No. 1, 1990, pp. 66–74.

[4]Hoeijmakers, H. W. M., "Modelling and Numerical Simulation of Vortex Flow in Aerodynamics," CP-494, Paper 1, AGARD, July 1991.

[5]de Laat, T. W. G., and Coene, R., "Two-Dimensional Vortex Motion in the Cross-Flow of a Wing-Body Configuration," *Journal of Fluid Mechanics*, Vol. 305, Dec. 1995, pp. 93–109.

[6]Bickley, W. G., "The Influence of Vortices upon the Resistance Experienced by Solids Moving Through a Liquid," *Proceedings of the Royal Society of London, Series A: Mathematical and Physical Sciences*, Vol. 119, 1928, pp. 146–156.

[7]Sarpkaya, T., "Lift, Drag, and Added-Mass Coefficients for a Circular Cylinder Immersed in a Time-Dependent Flow," *Journal of Applied Mechanics*, Vol. 30, March 1963, pp. 13–15.

[8]Lin, C. C., "On the Motion of Vortices in Two Dimensions—II Some Further Investigations on the Kirchhoff-Routh Function," *National Academy of Sciences*, Vol. 27, No. 12, 1941, pp. 575–577.

[9]Tomotika, S., and Sugawara, N., "Influence of Vortices upon the Resistance of a Circular Cylinder Moving Through a Fluid," *Proceedings of the Physico-Mathematical Society of Japan*, Vol. 20, No. 6, 1938, pp. 467–477.

[10]Milne-Thomson, L. M., *Theoretical Hydrodynamics*, 5th ed., Dover, Mineola, NY, 1996, pp. 173, 174, 369, 370.

[11]Saffman, P. G., *Vortex Dynamics*, Cambridge Univ. Press, New York, 1992, p. 43.

[12]Roy, D., "Resistance of a Circular Cylinder due to a Pair of Vortices Moving Symmetrically," *Zeitschrift für Angewandte Mathematik und Physik*, Vol. 10, No. 1, 1959, pp. 90–92.

[13]Lamb, H., *Hydrodynamics*, Dover, New York, 1932, p. 229.

[14]Brown, C. E., and Michael, W. E., "Effect of Leading-Edge Separation on the Lift of a Deltawing," *Journal of Aeronautical Sciences*, Vol. 21, Oct. 1954, pp. 690–694.

[15]Sacks, A. H., "Vortex Interference on Slender Airplanes," NACA TN 3525, Nov. 1955.

[16]Sacks, A. H., Lundberg, R. E., and Hanson, C. W., "A Theoretical Investigation of the Aerodynamics of Slender Wing-Body Combinations Exhibiting Leading-Edge Separation," NASA CR 719, March 1967.

[17]Sarpkaya, T., "An Inviscid Model of Two-Dimensional Vortex Shedding for Transient and Asymptotically Steady Separated Flow over an Inclined Plate," *Journal of Fluid Mechanics*, Vol. 68, Pt. 7, 1975, pp. 109–128.

A. Plotkin
Associate Editor